Smart Structures and Systems, *Vol. 28, No. 1 (2021) 89-104*
https://doi.org/10.12989/sss.2021.28.1.089

Damping enhancement of the inerter on the viscous damper in mitigating cable vibrations

Hui Gao [1], Hao Wang*[1], Jian Li [2], Zhihao Wang [3], Youhao Ni [1] and Ruijun Liang [1]

[1] *Key Laboratory of Concrete and Prestressed Concrete Structures of Ministry of Education, Southeast University, Nanjing 211189, China*
[2] *Department of Civil, Environmental and Architectural Engineering, The University of Kansas, Lawrence, KS 66045, USA*
[3] *School of Civil Engineering and Communication, North China University of Water Resources and Electric Power, Zhengzhou 450045, China*

(*Received July 11, 2020, Revised February 12, 2021, Accepted May 31, 2021*)

Abstract. This paper systematically investigates the effect of the inerter on the damping enhancement of a cable with a viscous damper (VD) installed close to the cable end. Three cases are considered, including the inerter installed parallel with the VD (PVID), the inerter placed in series with the VD (SVID), and the inerter installed at a higher location of the VD (HVID). The asymptotic solutions of the three cases are derived, which can predict the cable modal damping ratio when the inerter and the VD cause minimal perturbation in the undamped frequency of the cable. The effect of the inerter on the modal behavior of the cable with the VD is investigated. Based on the constrained static output LQR method, the effects of the inerter on the damping enhancement of the VD in mitigating cable multi-mode vibrations are further evaluated. The results show that the inerter can improve the control performance of the VD when the inertance is less than the optimum value. Further increasing the inertance beyond the optimum value, the optimum modal damping ratio of the cable decreases, and mode crossover is observed for the cable with PVID and HVID. Compared with the case where the VD and the inerter are located at the same location, the case of the HVID is more effective in mitigating cable multi-mode vibrations.

Keywords: damping enhancement; inerter; mode behavior; multi-mode vibration control; stay cable; viscous inerter damper

1. Introduction

Stay cables in cable-stayed bridges are often observed to experience excessive vibrations under external excitations (Ni *et al*. 2007, Li *et al*. 2013, Shen *et al*. 2018, Wang *et al*. 2020), such as wind, rain/wind, and traffic loadings. Frequent and excessive vibrations not only reduce the service life of cables but also have adverse effects on public confidence in the overall safety of the bridge. Various strategies have been adopted in real-world applications for the mitigation of cable vibrations, such as modification of the cable surface (Kleissl and Georgakis 2012), tying cables together (He *et al*. 2018), installing external dampers (Chen *et al*. 2004, Cai *et al*. 2007, Jamshidi *et al*. 2017, Zhou *et al*. 2018b, Liu *et al*. 2019), and using hybrid techniques (Ahmad *et al*. 2018).

Among these methods, the installation of passive viscous dampers (VD) near the cable-deck anchorage has received considerable attention. Kovacs (1982) first identified the optimum cable modal damping ratio based on the fixed-point method. Subsequently, Pacheco *et al*. (1993) proposed a universal estimation curve to design the VD for mitigating cable vibrations. Krenk (2000) developed an asymptotic solution to predict the cable modal damping ratio provided by the VD. The modal behavior of a cable with a VD was also systematically investigated (Main and Jones 2002). In addition, several methods and design tools have been developed to consider the effect of non-ideal factors on the damper performance and design parameters (Fujino and Hoang 2008, Fournier and Cheng 2014, Duan *et al*. 2019, Mehrabi and Tabatabai 1998), such as the cable sag and flexural stiffness, damper internal stiffness, support stiffness, nonlinearity, and the mass of the damper moving part. To design the damper for suppressing multi-mode cable vibrations, Wang *et al*. (2005) developed a suboptimal design procedure for the VD based on the optimal LQG control theory; Weber *et al*. (2009) presented a practical design method targeting at desired cable modes by constraining the minimum damping ratio of the cable. These results showed that the achievable modal damping of the cable is typically restricted by the small distance from the damper location to the cable anchorage compared with the total cable length. For long stay cables, it is challenging for the VD to provide enough damping to eliminate the cable vibrations.

To improve the control performance of the VD, semi-active dampers have been proposed and their superior performance has been proved both theoretically and experimentally (Johnson *et al*. 2003, Jung *et al*. 2004, Duan *et al*. 2005, Christenson *et al*. 2006, Kim *et al*. 2010, Huang *et al*. 2019a, Zhang *et al*. 2019, Jeong *et al*. 2019). However, passive control strategies are more preferred in

*Corresponding author, Professor,
E-mail: wanghao1980@seu.edu.cn

ISSN: 1738-1584 (Print), 1738-1991 (Online)

real-world applications. In view of this, passive negative stiffness dampers (NSD) have proposed (Chen *et al*. 2015, Shi *et al*. 2016, Zhou and Li 2016) to improve the VD performance inspired by the negative stiffness behavior of semi-active dampers (Li *et al*. 2008, Weber and Distl 2015). Chen *et al*. (2015) first demonstrated the advantages of the passive NSD in mitigating cable vibrations. Shi *et al*. (2016) investigated the dynamic behavior of cable with NSD. Furthermore, the pre-spring NSD (Zhou and Li 2016) and the magnetic induced NSD (Shi *et al*. 2017) were invented to validate the NSD performance experimentally. Based on the refined design formula, the performance of the NSD in mitigating cable multi-mode vibrations was also evaluated (Javanbakht *et al*. 2020).

Recently, inerter-based dampers have gained extensive attention due to their ability to enhance damping which is similar to the NSD (Ikago *et al*. 2012, Lazar *et al*. 2014, Nakamura *et al*. 2014, Marian and Giaralis 2014, Hu *et al*. 2015, Giaralis and Petrini 2017, Zhu *et al*. 2019, Domenico and Ricciardi 2019, Ma *et al*. 2020, 2021, Zhang *et al*. 2020). Lazar *et al*. (2016) first reported the effectiveness of the tuned inerter damper (TID) in controlling single mode cable vibrations. Sun *et al*. (2017) investigated the combined effect of the TID and cross-ties for cable vibration control. Lu *et al*. (2017, 2019) evaluated the control performance of the paralleled viscous inerter damper (PVID) and found that a significant damping improvement can be achieved for a specific cable mode compared to the VD. Shi and Zhu (2008) proposed an optimum design method to design the PVID for suppressing cable vibrations. Based on their designed electromagnetic PVID, Li *et al*. (2019), Wang *et al*. (2019) and Li *et al*. (2020) experimentally proved the superior performance of the PVID for cable vibration control. The comparative study of typical inerter-based dampers for cable vibration control was also reported (Luo *et al*. 2019, Huang *et al*. 2019b, Chen *et al*. 2021). The results showed that the inerter-based dampers are more effective than the VD in mitigating cable vibrations.

However, the above studies mainly focus on the scenario in which the damper and the inerter are installed at the same location. A recent study showed that a concentrated mass placed at a higher location than the VD can achieve better control performance compared with the case when they are located together (Zhou *et al*. 2018a). But the mass may be too large to make a significant increment on the cable modal damping ratio. Compared with the concentrated mass, the inerter can generate an inertial mass that is thousands of times its physical mass while being installed close to the cable end for aesthetic and practical reasons. Nonetheless, the dynamic behavior for the inerter installed at a higher location of the VD has not been investigated. To inquire into the effect of the inerter on the damping enhancement of the VD in mitigating cable vibrations, the modal behavior of the cable-VD-inerter system is systematically investigated. Three cases are considered, including 1) the inerter is installed parallel to the VD (i.e., PVID), 2) the inerter is placed in series with the VD (SVID), and 3) the inerter is installed at a higher location than the VD (HVID). The asymptotic solution for the VD and the inerter installed close to the cable end is derived. In addition, the effects of the inerter on the cable oscillation frequency, the optimum modal damping ratio, and the control performance in mitigating multi-mode cable vibrations are evaluated.

2. General problem formulation

Fig. 1 shows the unified analytical model to evaluate the effect of the inerter on the modal behavior of a cable with a VD installed close to the cable end, where T, m and l denote the tension force, the mass per unit length and the length of the cable, respectively. Some minor but important factors on the modal behavior are neglected, such as the inherent damping, the sag and the flexural stiffness of the cable, the damper stiffness and support stiffness, as the effect of the inerter is the focus of this study. The equation of the transverse motion of the cable is expressed as (Hoang and Fujino 2008)

$$T\frac{\partial^2 u(x,t)}{\partial x^2} - m\frac{\partial^2 u(x,t)}{\partial t^2} = f_1(t)\delta(x-x_1) + f_2(t)\delta(x-x_2) \tag{1}$$

with the boundary condition

$$u(0,t) = u(l,t) = 0 \tag{2}$$

where x is the location coordinate along the cable; $u(x,t)$is the transverse displacement of the cable at the location x and the time t; $\delta(\cdot)$ is the Dirac delta function; $f_1(t)$ and $f_2(t)$ denote the transverse force applied to the cable, which are expressed in Table 1 for the three cases considered in this study.

For free vibration, the cable transverse displacement $u(x,t)$ and damper forces, $f_1(t)$ and $f_2(t)$, can be assumed respectively as

$$u(x,t) = Re[\,U(x)e^{i\omega t}]$$
$$f_1(t) = Re[\,F_1 e^{i\omega t}],\ f_2(t) = Re[\,F_2 e^{i\omega t}] \tag{3}$$

where $i=\sqrt{-1}$; ω and $U(\mathrm{x})$ are the complex eigen frequency and the corresponding complex mode shape of the cable, respectively; F_1 and F_2 denote the amplitude of the damper force, respectively.

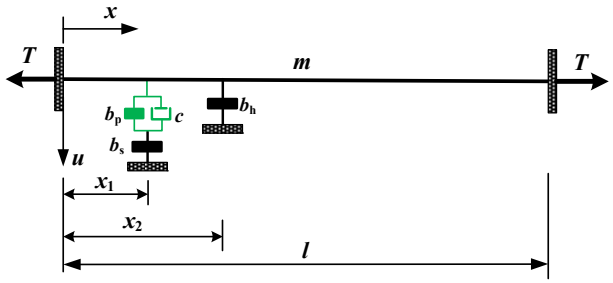

Fig. 1 The unified analytical model a taut cable with inerter and VD

Table 1 The transverse force applied to the cable

Case	Description	$f_1(t)$	$f_2(t)$
PVMD	$b_s = 0$ $b_h = 0$	$b_p\ddot{u}(x_1,t) + c\dot{u}(x_1,t)$	0
SVMD	$b_p = 0$ $b_h = 0$	$b_s\ddot{u}_b(t)$ or $c[\dot{u}(x_1,t) - \dot{u}_b(t)]$	0
HVMD	$b_p = 0$ $b_s = 0$	$c\dot{u}(x_1,t)$	$b_h\dot{u}(x_1,t)$

*Note: b_p, b_s, and b_h denote the inertance of the inerter for the case PVID, SVID, and HVID, respectively; $\ddot{u}_b(t)$ in case 2 denotes the velocity of the inerter in the SVID.

Substituting Eq. (3) into Eq. (1), $U(x)$ should satisfy the following equation

$$\frac{d^2U(x)}{dx^2} + \beta^2 U(x) = 0 \qquad \begin{cases} 0 \le x \le x_1 \\ x_1 \le x \le x_2 \\ 0 \le x^* \le x_2^* \end{cases} \tag{4}$$

where $\beta = \omega\sqrt{m/T}$ refers to the wavenumber, and $x_1^* = l - x_1, x_2^* = l - x_2$.

Considering the boundary conditions shown in Eq. (2) at cable ends, the compatibility conditions in Eq. (5)

$$U(x_1^-) = U(x_1^+) = U(x_1), U(x_2^-) = U(x_2^+) = U(x_2),$$
$$T\left(\left.\frac{dU(x)}{dx}\right|_{x_j^+} - \left.\frac{dU(x)}{dx}\right|_{x_j^-}\right) = F_j, j=1, 2 \tag{5}$$

the solution of Eq. (4) is derived as

$$U(x) = \begin{cases} U(x_1)\dfrac{\sin\beta x}{\sin\beta x_1} & 0 \le x \le x_1 \\ U(x_1)\dfrac{\sin\beta(x_2 - x)}{\sin\beta(x_2 - x_1)} + U(x_2)\dfrac{\sin\beta(x - x_1)}{\sin\beta(x_2 - x_1)} & x_1 \le x \le x_2 \\ U(x_2)\dfrac{\sin\beta x^*}{\sin\beta x_2^*} & 0 \le x^* \le x_2^* \end{cases} \tag{6}$$

where the wavenumber β is satisfied as

$$\left(cot\,\beta\,x_1 + \frac{\frac{F_1}{T}}{\beta U(x_1)}\right)\left(cot\,\beta\,x_2^* + \frac{\frac{F_2}{T}}{\beta U(x_2)}\right) + \left(cot\,\beta\,x_1 + \frac{\frac{F_1}{T}}{\beta U(x_1)} + cot\,\beta\,x_2^* + \frac{\frac{F_2}{T}}{\beta U(x_2)}\right)cot\,\beta\,(x_2 - x_1) = 1 \tag{7}$$

Substituting $f_1(t)$ and $f_2(t)$ shown in Table 1 into Eq. (7), the wave numbers determinant equation for the three cases can be further expressed in Eq. (8) and can be numerically solved by using the Newton's method.

$$tan\,\beta\,l = \frac{A_\tau + iB_\tau}{C_\tau + iD_\tau}, \qquad \tau = p, \mathrm{s}, \mathrm{h} \tag{8}$$

For the cable with the PVID

$$\begin{aligned} &A_p = -\chi_p\,sin^2\,\beta\,x_1 \qquad B_p = \eta\,sin^2\,\beta\,x_1 \\ &C_p = 1 - \chi_p\,sin\,\beta\,x_1\,cos\,\beta\,x_1 \quad D_p = \eta\,sin\,\beta\,x_1\,cos\,\beta\,x_1 \end{aligned} \tag{8a}$$

For the cable with the SVID

$$\begin{aligned} &A_s = 0 \qquad B_s = \eta\sin^2\beta x_1 \\ &C_s = 1 \qquad D_s = \eta\sin\beta x_1\cos\beta x_1 - \eta/\chi_s \end{aligned} \tag{8b}$$

For the cable with the HVID

$$\begin{aligned} &A_h = -\chi_h\,sin^2\,\beta\,x_2 \\ &B_h = \eta\,sin^2\,\beta\,x_1 - \chi_h\eta\,sin\,\beta\,x_1\,sin\,\beta\,x_2\,sin\,\beta\,(x_2 - x_1) \\ &C_h = 1 - \chi_h\,sin\,\beta\,x_2\,cos\,\beta\,x_2 \\ &D_h = \eta\,sin\,\beta\,x_1\,cos\,\beta\,x_1 - \chi_h\eta_1\,sin\,\beta\,x_1\,cos\,\beta\,x_2\,sin\,\beta\,(x_2 - x_1) \end{aligned} \tag{8c}$$

in which

$$\chi_\tau = \frac{b_\tau\omega}{\sqrt{mT}}, \quad \eta = \frac{c}{\sqrt{mT}}, \quad \tau = p, \mathrm{s}, \mathrm{h} \tag{9}$$

3. Asymptotic solution for small frequency shifts

As both the VD and the inerter have two connection points, they should be installed closed to the cable-deck anchorage in real-word applications. In this study, the locations of the VD, x_1 and the inerter location, x_2 are assumed as

$$x_1/l \le x_2/l \le 5\% \tag{10}$$

When the inertance is small, the installation of the VD and the inerter could only cause minimal perturbation in the wave numbers of the lower cable modes, and the following approximations for the n^{th} cable mode can be obtained

$$\begin{aligned} &\beta_n^0 \simeq \frac{n\pi}{l};\ tan\,\beta_n\,l \simeq \beta_n l - \beta_n^0 l;\ sin\,\beta_n\,x_1 \simeq \beta_n^0 x_1; \\ &sin\,\beta_n\,x_2 \simeq \beta_n^0 x_2;\ sin\,\beta_n\,(x_2 - x_1) \simeq \beta_n^0(x_2 - x_1); \\ &cos(\beta_n x_1) \simeq cos(\beta_n x_2) \simeq 1 \end{aligned} \tag{11}$$

Substituting Eq. (11) into Eq. (8), the solution of wave numbers β_n of the n^{th} cable mode can be obtained. Subsequently, the natural frequency of the cable ω_n can be expressed as (Krenk 2000)

$$\omega_n = \beta_n\sqrt{T/m} = |\omega_n|(\sqrt{1 - \zeta_n^2} + i\zeta_n) \tag{12}$$

where the real part of the natural frequency denotes the oscillatory frequency of the cable; ζ_n is the n^{th} cable modal damping ratio and can be solved as

$$\zeta_n = \frac{Im(\omega_n)}{|\omega_n|} = \frac{Im(\beta_n)}{|\beta_n|} \approx \frac{Im(\Delta\beta_n)}{|\beta_n^0|} \tag{13}$$

For the cable with the PVID, Wang *et al*. (2019) has established the asymptotic solution to describe the cable modal behavior. For the completeness, the results are introduced in this study. The dimensionless natural frequency $\bar{\omega}$, the n^{th} modal damping ratio ζ_n, the optimum damping coefficient c_n^{opt} and the corresponding optimum modal damping ratio ζ_n^{opt} for a certain inertance can be expressed as Wang *et al*. (2019)

$$\begin{aligned}
\bar{\omega} &= \frac{\omega_n}{\omega_n^0} = 1 + \frac{-\bar{b}_{\mathrm{p},n}(1-\bar{b}_{\mathrm{p},n}) + \bar{c}_n^2}{(1-\bar{b}_{\mathrm{p},n})^2 + \bar{c}_n^2} \\
&\quad + \frac{i\bar{c}_n}{(1-\bar{b}_{\mathrm{p},n})^2 + \bar{c}_n^2}\frac{x_1}{l} \\
\zeta_n &= \frac{\bar{c}_n/(1-\bar{b}_{\mathrm{p},n})}{1+\left[\bar{c}_n/(1-\bar{b}_{\mathrm{p},n})\right]^2}\frac{1}{(1-\bar{b}_{\mathrm{p},n})}\frac{x_1}{l} \\
c_n^{\text{opt}} &= \frac{\left|1-\bar{b}_{\mathrm{p},n}\right|T}{\omega_n^0 x_1},\ \zeta_n^{\text{opt}} = \frac{1}{\left|1-\bar{b}_{\mathrm{p},n}\right|}\frac{x_1}{2l}
\end{aligned} \tag{14}$$

where $\bar{b}_{\tau,n} = \chi_\tau \beta_n^0 x_1$, $\tau = \mathrm{p}, \mathrm{s}$, and $\bar{c}_n = \eta\beta_n^0 x_1$ denote dimensionless inertance and damping coefficient, respectively.

Fig. 2 shows the frequency-modal damping ratio curves, damping coefficient-modal damping ratio curves, and the inertance-modal damping ratio curves of the cable with PVID. As shown in Fig. 2(a), the inerter would decrease the cable undamped oscillatory frequency. However, the cable clamped frequency, the frequency when the damping coefficient is increased to infinity, is unaffected by the inerter. Figs. 2(b) and (c) indicate that the inerter could increase the optimum modal damping ratio of the cable and decrease the optimum damping coefficient of the VD. Hence, PVID is a more economical and effective strategy for cable vibration control than the VD. The comparison between the asymptotic solution and numerical solution shows that the asymptotic solution can well predict the maximum modal damping ratio of the cable (the maximum error is less than 15%) when the dimensionless inertance is less than 0.820 but begins to lose its accuracy with the inertance further increasing. The above results for cable vibration with the PVID are consistent with that reported in Shi and Zhu (2018) and Wang *et al*. (2019).

For the cable with the SVID, the dimensionless natural frequency can be derived as

$$\begin{aligned}
\bar{\omega} &= \frac{\omega_n}{\omega_n^0} = 1 + \frac{i\bar{c}_n}{1+i\left(\bar{c}_n - \frac{\bar{c}_n}{\bar{b}_{\mathrm{s},n}}\right)}\frac{x_1}{l} \\
&= 1 + \frac{\bar{c}_n^2\left(1-\frac{1}{\bar{b}_{\mathrm{s},n}}\right)}{1+\bar{c}_n^2(1-1/\bar{b}_{\mathrm{s},n})^2}\frac{x_1}{l} \\
&\quad + \frac{i\bar{c}_n}{1+\bar{c}_n^2(1-1/\bar{b}_{\mathrm{s},n})^2}\frac{x_1}{l}
\end{aligned} \tag{15}$$

Substituting the Eq. (15) into Eq. (13), the n^{th} modal damping ratio of the cable can be derived as

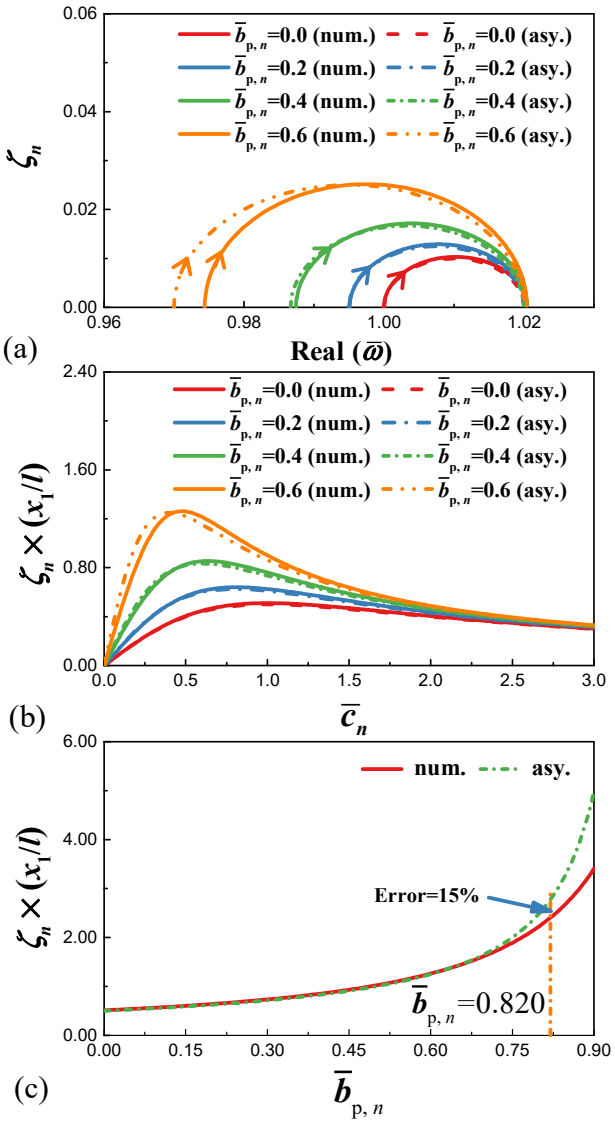

Fig. 2 The frequency-modal damping ratio curves, the damping coefficient -modal damping ratio curves, and the inertance coefficient-modal damping ratio curves of the cable with PVID ($x_1 = 0.02l$)

$$\zeta_n = \frac{\bar{c}_n}{1+(\bar{c}_n - \bar{c}_n/\bar{b}_{\mathrm{s},n})^2}\frac{x_1}{l} = \frac{\bar{c}_n}{1+\bar{c}_n^2(1-1/\bar{b}_{\mathrm{s},n})^2}\frac{x_1}{l} \tag{16}$$

The optimum damping coefficient of the SVID can be obtained by

$$\frac{\partial\zeta_n}{\partial c} = \frac{\partial\zeta_n}{\partial\bar{c}_n}\cdot\frac{\partial\bar{c}_n}{\partial c} = 0 \tag{17}$$

leading to the value

$$c_n^{\text{opt}} = \frac{T}{\left|1-1/\bar{b}_{\mathrm{s},n}\right|\omega_n^0 x_1} \tag{18}$$

Substituting Eq. (18) into Eq. (16), the optimum modal damping ratio is expressed as

$$\zeta_n^{\text{opt}} = \frac{1}{2}\frac{1}{\left|1-1/\bar{b}_{\mathrm{s},n}\right|}x_1/l \tag{19}$$

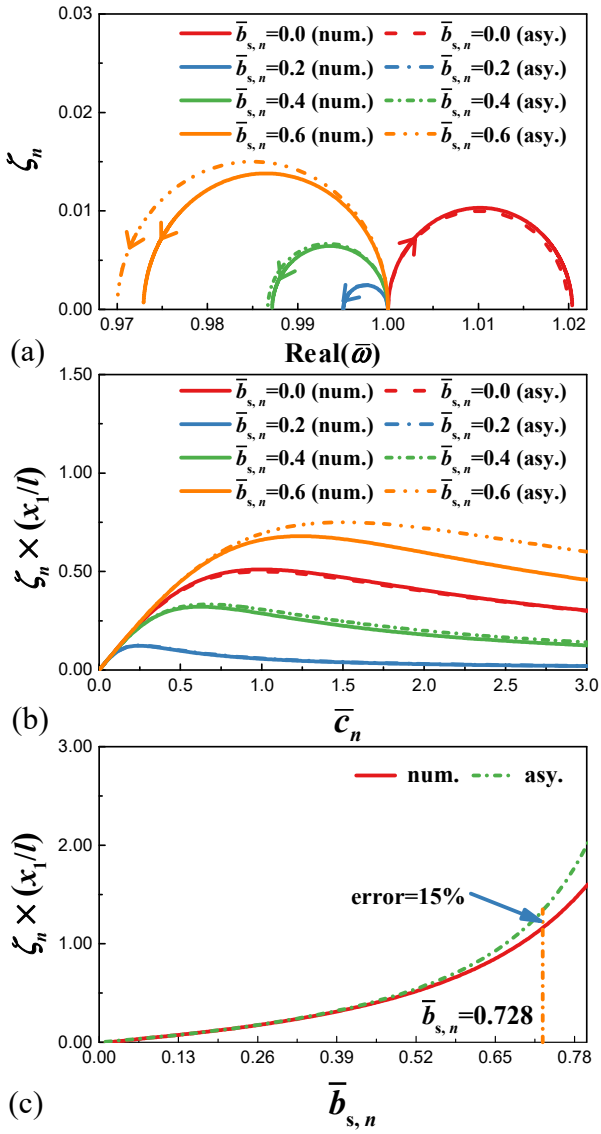

Fig. 3 The frequency-modal damping ratio curves, the damping coefficient -modal damping ratio curves, and the inertance-modal damping ratio curves of the cable with SVID ($x_1 = 0.02l$)

According to Eqs. (19)-(20), we can obtain

$$\begin{cases} c_n^{\text{opt}} \le \dfrac{T}{x_1\omega_n^0} & \zeta_n^{\text{opt}} \le \dfrac{x_1}{2l} \quad 0 < \bar{b}_{s,n} \le 0.5 \\ c_n^{\text{opt}} > \dfrac{T}{x_1\omega_n^0} & \zeta_n^{\text{opt}} > \dfrac{x_1}{2l} \quad \bar{b}_{s,n} > 0.5 \text{且} \bar{b}_n \ne 1 \\ c_n^{\text{opt}} = \dfrac{T}{x_1\omega_n^0} & \zeta_n^{\text{opt}} = \dfrac{x_1}{2l} \quad \bar{b}_{s,n} \gg 1 \end{cases} \tag{20}$$

Eq. (16) indicates that the inerter only affects the cable clamped frequency while hardly affects the cable undamped oscillatory frequency. The clamped frequency decreases with the increase of the inertance when the dimensionless inertance is less than 1. In addition, the SVID will be degraded to the VD when the inertance increases to infinity. Eq. (20) implies that the inerter in the SVID has an adverse effect on the performance of the VD when the dimensionless inertance is less than 0.5. When the dimensionless inertance is larger than 0.5, the inerter can promote the efficiency of the VD while also increase its optimum damping coefficient. The above results can also be observed in Fig. 3, which plots the frequency-modal damping ratio curves, the damping coefficient-modal damping ratio curves, and the inertance-modal damping ratio curves of the cable with SVID. Similar to the cable with the PVID, the asymptotic solution agrees well with the numerical solution for small inertance and the error of the asymptotic solution is less than 15% when $\bar{b}_n < 0.728$.

For the cable with the HVID, the dimensionless natural frequency can be derived as

$$\bar{\omega} = \frac{\omega_n}{\omega_n^0} = 1 + \frac{-\bar{b}_{h,n}\frac{x_2^2}{x_1^2} + i\bar{c}_n\left[1 - \bar{b}_{h,n}\frac{x_2}{x_1}\left(\frac{x_2}{x_1} - 1\right)\right]}{1 - \bar{b}_{h,n}\frac{x_2}{x_1} + i\bar{c}_n\left[1 - \bar{b}_{h,n}\left(\frac{x_2}{x_1} - 1\right)\right]}\frac{x_1}{l} \tag{21}$$

The n^{th} modal damping ratio of the cable with the HVID can be further derived by substituting Eq. (21) into Eq. (13), yields

$$\begin{aligned} \zeta_n &= \frac{Im(\Delta\beta_n)}{|\beta_n^0|} \\ &= \frac{\bar{c}_n}{\left(1 - \bar{b}_{h,n}\frac{x_2}{x_1}\right)^2 + \bar{c}_n^2\left[1 - \bar{b}_{h,n}\left(\frac{x_2}{x_1} - 1\right)\right]^2}\frac{x_1}{l} \end{aligned} \tag{22}$$

Substituting the Eq. (22) into Eq. (17), the optimum damping coefficient of the VD is expressed as

$$c_n^{\text{opt}} = \frac{\left|1 - \bar{b}_{h,n}\frac{x_2}{x_1}\right| T}{\left|1 - \bar{b}_{h,n}\left(\frac{x_2}{x_1} - 1\right)\right| \omega_n x_1} \tag{3}$$

The n^{th} optimum modal damping ratio of the cable can be obtained by substituting the Eq. (23) into Eq. (22), and it is expressed as

$$\zeta_n^{\text{opt}} = \frac{1}{2}\frac{1}{\left(1 - \bar{b}_{h,n}\frac{x_2}{x_1}\right)\left[1 - \bar{b}_{h,n}\left(\frac{x_2}{x_1} - 1\right)\right]}\frac{x_1}{l} \tag{24}$$

Fig. 4 shows the frequency-modal damping ratio curves and damping coefficient-modal damping ratio curves for the cable with HVID. As shown in Fig. 4(a), the cable undamped oscillatory frequency and clamped frequency decrease as the inertance increases. Compared with the cable clamped frequency, the inerter has greater impact on the cable undamped frequency. This phenomenon can be explained by Fig. 5, which gives the special case of the cable with the HVID. When the damping coefficient of the VD increases to the infinity, the cable with the HVID in Fig. 5(b) evolves into Fig. 5(c). The inerter location in the large segment of the cable is smaller than the case when the damping coefficient equals to zero in Fig. 5(a). Similar to the cable with the PVID, Fig. 4(b) shows that the inerter could promote the efficiency of the VD. As the inertance increases, the optimum damping ratio also increases, while the corresponding optimum damping coefficient slightly

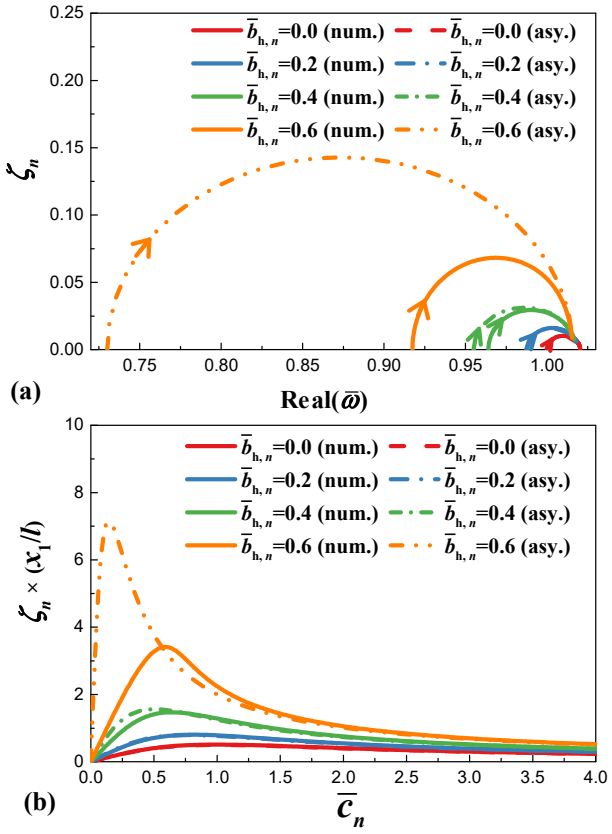

Fig. 4 The frequency-modal damping ratio curves and the damping coefficient-modal damping ratio curves of the cable with HVID ($x_1 = 0.02l), x_2 = 0.03l$)

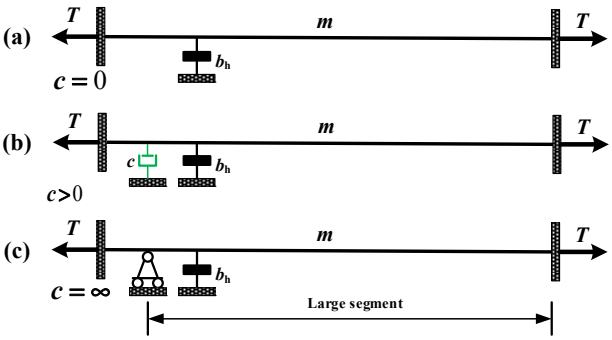

Fig. 5 The special case of the cable with the HVID

decreases at first and then increases with the further increase of the inertance.

Fig. 6 further plots the frequency-modal damping ratio curves, damping coefficient-modal damping ratio curves for several inerter locations of the cable with HVID when the dimensionless inertance of the inerter is equal to 0.2. As show in Fig. 6(a), both the cable undamped oscillatory frequency and clamped frequency decrease with the increase of the inerter location. Compared with the cable undamped oscillatory frequency, the inerter location has less impact on the cable clamped frequency. Fig. 6(b) shows that the optimum modal damping ratio of the cable and the corresponding optimum damping coefficient of the VD increase with the increase of the inerter location.

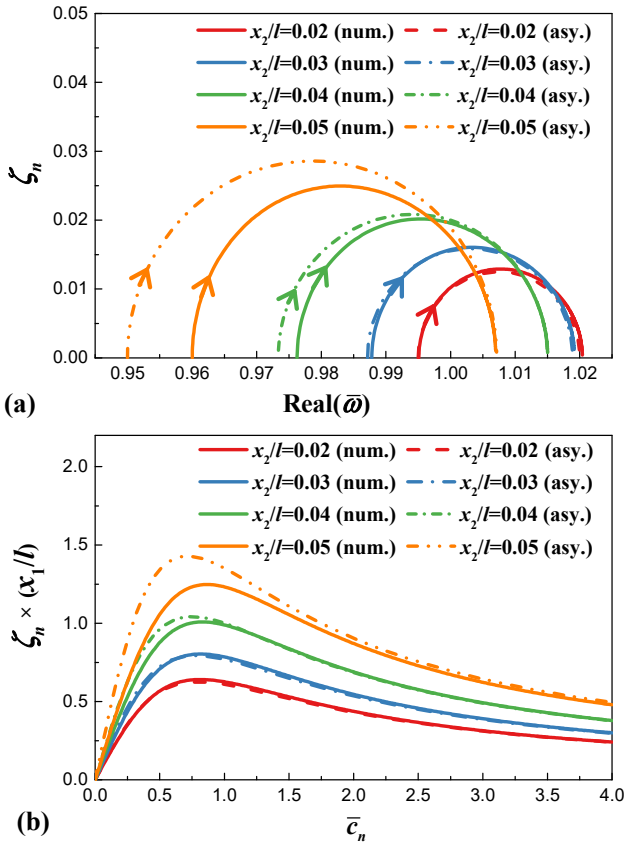

Fig. 6 The frequency-modal damping ratio curves and the damping coefficient-modal damping ratio curves of the cable with HVID ($x_1 = 0.02l$, $\bar{b}_{h,n} = 0.2$)

Fig. 7 further compares the asymptotic and numerical solution of the maximum modal damping ratio of the cable with HVID. When the error of the approximate solution reaches 15%, the dimensionless inertance are respectively equals to 0.470 ($x_2/l = 0.03$), 0.296 ($x_2/l = 0.04$), and 0.202 ($x_2/l = 0.05$). Further increasing the inertance, the asymptotic solution begins to lose its accuracy. This implies that a smaller inertance could cause the asymptotic solution to loss its accuracy when the inerter is installed at a higher location than the VD.

4. Modal behavior for large frequency shifts

Previous studies have shown that the cable modal behavior is dependent on the damper location (Main and Jones 2002, Hoang and Fujino 2008, Zhou *et al*. 2018a) and the inertance of the inerter (Shi and Zhu 2018). To focus on the effect of the inerter on the modal behavior of the cable, the location of the VD of three cases is assumed to be 2%l from the cable end, and the inerter in HVID is installed at 3%l from the cable end.

4.1 Modal behavior of the cable with PVID

Shi and Zhu (2018) has investigated the modal behavior of the cable with PVID, and observed the phenomenon of cable mode crossover at the optimal inertance. On this

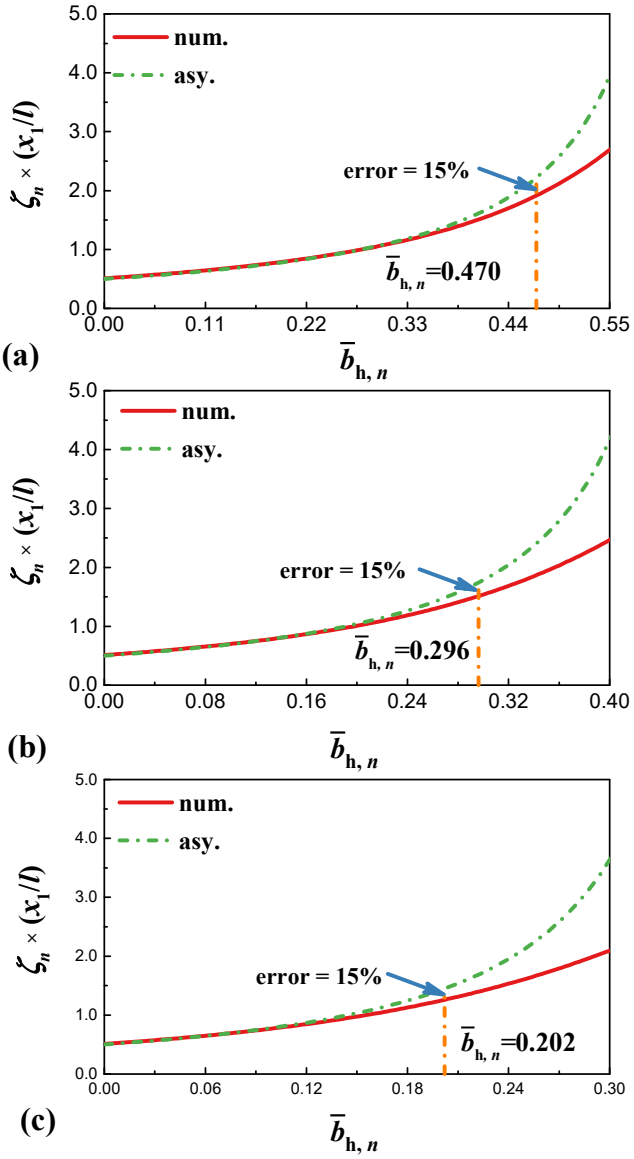

Fig. 7 The asymptotic and numerical solutions of the maximum modal damping ratio of the cable with HVID (a) $x_2/l = 0.03$; (b) $x_2/l = 0.04$; (c) $x_2/l = 0.05$

basis, this study systematically investigates the effect of the inerter on the modal behavior of the cable with PVID, and found the modal behavior of the cable can be divided into three distinct regimes. The characteristics of the three regimes are described as follows:

(1) Regime 1 (underdamped modes): when $0 \le b_p < \bar{b}_{p,n}^{opt} T/(\omega_n^0 x_1)$, where the optimum dimensionless inertance $\bar{b}_{p,n}^{opt}$ can be obtained by the optimum procedure in Shi and Zhu (2018). In this regime, as the inertance increases, the cable undamped frequency decreases, while the optimum cable modal damping ratio increases.

(2) Regime 2 (subcritical damped modes): when $\bar{b}_{p,n}^{opt} T/(\omega_n^0 x_1) \le b_p < \bar{b}_{p,n-1}^{opt} T/(\omega_{n-1}^0 x_1)$, the frequency-damping evolution curves originate from the undamped cable frequency, and approach the critical damping as $\eta \to \eta_{cr}$. The determination equation of the critical value η_{cr} is given in the appendix. When $\eta \ge \eta_{cr}$, $\mathrm{Real}(\omega_n) = 0$ and $\zeta_n = 1$, non-oscillatory decay is found. The cable mode is translated into the overdamped mode. In this regime, mode crossover is observed, in which the cable vibration in the n^{th} cable mode is covered by the $(n+1)^{th}$ cable mode with limited damping.

(3) Regime 3 (underdamped modes): when $b_p \ge \bar{b}_{p,n-1}^{opt} T/(\omega_{n-1}^0 x_1)$, the frequency-damping evolution curves originate from the undamped frequency of the n^{th} cable mode, and terminate at the clamped frequency of the $(n-1)^{th}$ cable mode. The n^{th} mode cable vibration is translated into the $(n-1)^{th}$ cable mode, and the optimum modal damping ratio decreases as the inertance increases.

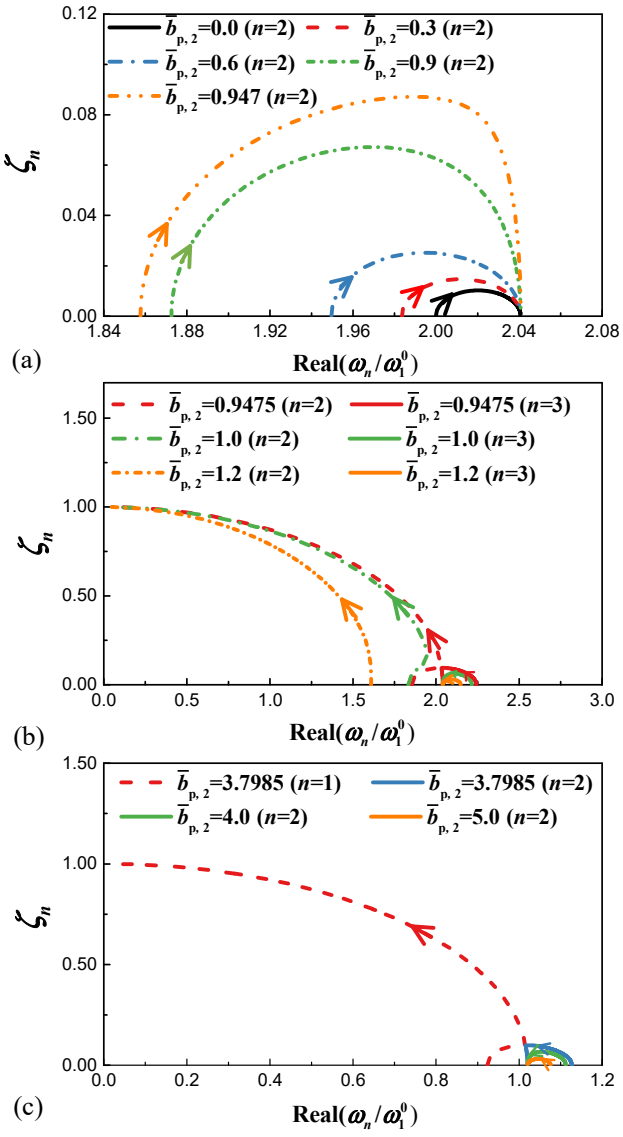

Fig. 8 Frequency-damping evolution curves of the cable with PVID in the n^{th} cable mode (a) regime 1; (b) regime 2; (c) regime 3

As an example, Fig. 8 shows the frequency-damping evolution curves of the cable with the PVID in the 2nd cable mode. Fig. 8(a) shows that the characteristics of the frequency-damping evolution curves in regime 1 are similar to those previously discussed in Fig. 2(a). Each curve originates from the second undamped frequency, and terminates at the second clamped frequency. Due to the effect of the inerter, the dimensionless undamped cable frequency decreases with the increase of the inertance, while the dimensionless clamped frequency is independent on the inerter and approximately equals to $2l/(l-x_1)$. The optimum cable modal damping ratio increases as the inertance increases in this regime.

As shown in Fig. 8(b), mode crossover begins to occur at the second and the third cable mode when $b_p = \bar{b}_{p,2}^{opt} T/(\omega_2^0 x_1)$, where $\bar{b}_{p,2}^{opt} = 0.9475$. The frequency-damping evolution curves of the second and third mode move towards each other as the damping coefficient increases and meet each other at the optimum damping coefficient of the 2nd cable mode. When the damping coefficient increases beyond the optimum value, the second modal damping ratio increases monotonically and $\zeta_2 \to 1$ when $\eta \to \eta_{cr}$, while the third modal damping ratio decreases monotonically and $\zeta_3 \to 0$ when $\eta \to \infty$. When the inertance is larger than the optimum value, as the damping coefficient increases, the second modal damping ratio increases monotonically and terminates at 1 when $\eta \geq \eta_{cr}$. However, the cable oscillation frequency decreases monotonically and terminates at 0 when $\eta \geq \eta_{cr}$. The frequency-damping evolution curves in the third mode originate from its undamped frequency and terminate at the clamped frequency of the second mode. Due to the effect of the inerter, the undamped cable frequency and optimum modal damping ratio in the third mode decrease as the inertance increases. Considering that the second modal damping ratio of the cable is much larger than that of the third mode, the actual vibration of the second cable mode is fully concealed by the third mode with a limited damping ratio.

As shown in Fig. 8(c), mode crossover begins to occur at the second and the first cable mode when $b_p = \bar{b}_{p,1}^{opt} T/(\omega_1^0 x_1)$, where $\bar{b}_{p1}^{opt} T/(\omega_1^0 x_1)$ is equal to $3.7985T/(\omega_2^0 x_1)$. The frequency-damping evolution curves in the second mode originate from its undamped frequency and terminate at the clamped frequency of the first mode. The first modal damping ratio increases monotonically with the damping coefficient of the VD and $\zeta_1 = 1$ when $\eta \geq \eta_{cr}$. The second mode cable vibration has been translated into the first mode vibration.

Fig. 9 shows the mode shapes of the 2nd cable mode for several inertance values when $\bar{c} = 0.5$. As shown in Fig. 9(a), the mode shape amplitude at the VD location in regime 1 increases with the increase of the inertance. This can enhance the energy dissipation efficiency of the VD (Lu *et al*. 2017, Shi and Zhu 2018, Li *et al*. 2019, Wang *et al*. 2019), which agrees well with the damping enhancement discussed in Fig. 8(a).

For the mode shapes in regime 2 shown in Fig. 9(b), the mode shape of the second mode becomes the hybrid curve of a sine and a hyperbolic sine function, which corresponds

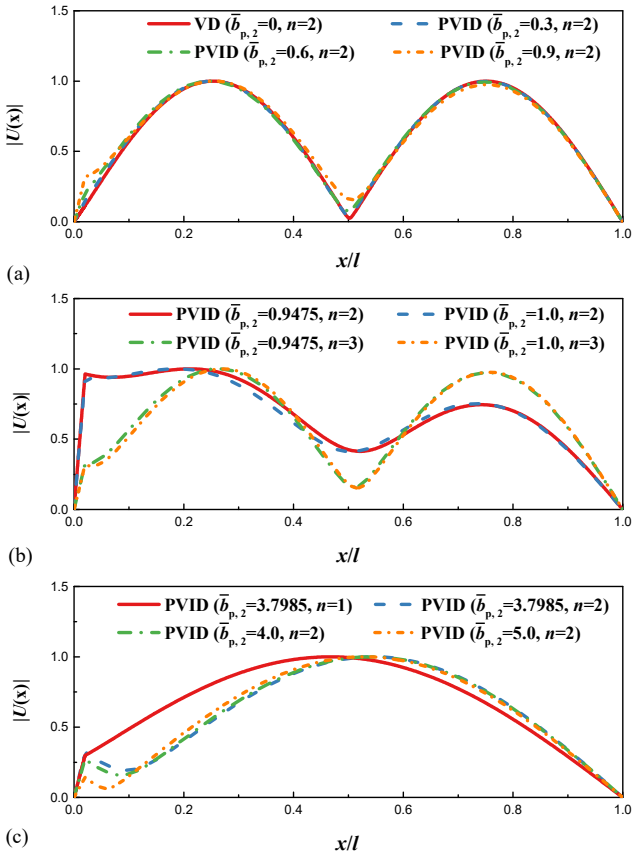

Fig. 9 Mode shapes of cable with PVID in the 2nd mode (a) regime 1; (b) regime 2; (c) regime 3

to the modal behavior of the subcritical damped modes. The mode shapes of the third mode are similar to the second mode of the free cable, which implies that mode crossover occurred in this regime. In addition, the mode shape amplitude at the VD location of the third mode decreases as the inertance increases, indicating that the cable's modal damping ratio would decreases with the increase of the inertance.

For the mode shapes in regime 3 shown in Fig. 9(c), the mode shape of the second mode is similar to the first mode of the free cable, which implies that the second mode vibration of cable with PVID is converted as the first mode vibration. The mode shape amplitude at the VD location of the second mode decreases as the inertance increases, indicating that the inerter would decrease the cable's first modal damping ratio.

4.2 Modal behavior of the cable with SVID

Unlike the modal behavior of the cable with PVID, there are only two distinct regimes of the cable with SVID observed in the n^{th} cable mode with the variation of the inertance.

(1) Regime 1 (underdamped modes): when $0 \leq b_s < \bar{b}_{s,n}^{opt} T/(\omega_n^0 x_1)$, the undamped cable frequency is hardly affected by the inerter. As the inertance increases, the clamped cable frequency decreases,

while the optimum cable modal damping ratio increases.

(2) Regime 2 (underdamped modes): when $b_s \geq \bar{b}_{s,n}^{opt} T/(\omega_n^0 x_1)$, both the cable clamped frequency and optimum modal damping ratio decrease as the inertance increases.

Above results can be seen in Fig. 10, which shows the frequency-damping evolution curves of the cable with the SVID in the second cable mode. It is seen from Fig. 10 that:

(1) when $\bar{b}_{s,2} \leq 1.047$, the frequency-damping evolution curves originate from the undamped oscillation frequency towards the left as the damping coefficient increases. It is because the inerter would decrease the clamped cable frequency while hardly affecting the undamped frequency. The optimum cable modal damping ratio increases with the increase of the inertance. However, the SVID provides less damping to cable than the VD when the dimensionless inertance is less than 0.5.

(2) When $\bar{b}_{s,2} \geq 1.048$, the clamped cable frequency is larger than that of the cable with the VD due to the effect of the inerter. The frequency-damping evolution curves move from the undamped oscillation frequency towards right as the damping coefficient increases. With the increase of the inertane, both the clamped frequency and the optimum modal damping ratio decrease. But the cable's optimum modal damping ratio is always larger than that with the VD.

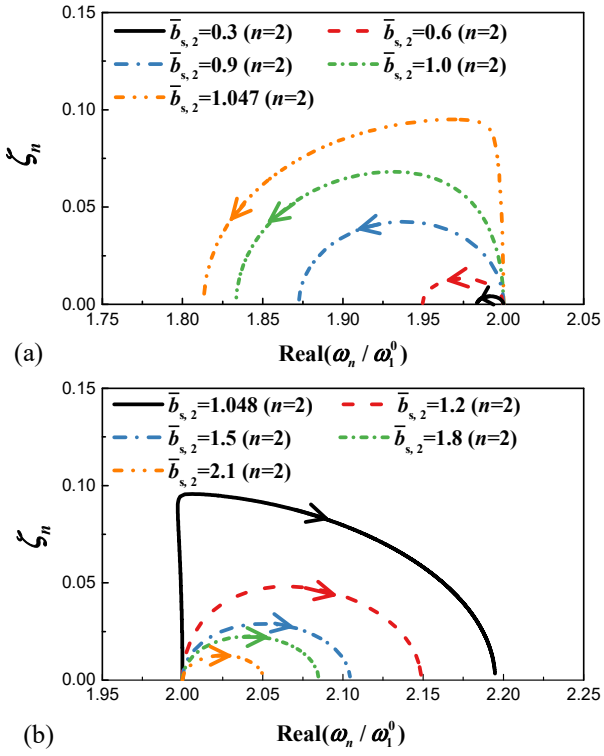

Fig. 10 Frequency-damping evolution curve of the cable with SVID in the n^{th} cable mode (a) regime 1; (b) regime 2.

Fig. 11 shows the mode shapes in the 2nd cable mode for several inertance values when $\bar{c} = 2.0$. As shown in Fig. 11(a), the mode shape amplitude at the damper location in regime 1 increases with the increase of the inertance. By solving the equation $b_s[\ddot{u}(x_1) - \ddot{u}_c] = c\dot{u}_c$, the vibration amplitude of the VD in the SVID can be obtained by

$$\tilde{u}_c = \sqrt{\frac{1}{1+4\xi_d^2}}\tilde{u}(x_1) \tag{25}$$

where $\ddot{u}(x_1)$ denotes the acceleration of the SVID, $\dot{u}_c$ and $\ddot{u}_c$ denote the velocity and the acceleration of the VD, respectively; $\tilde{u}_c$ and $\tilde{u}(x_1)$ represent the displacement amplitude of VD and SVID, respectively; and $\xi_d = c/(2b_s\omega_n^0)$.

Eq. (25) indicates that increasing the displacement of the SVMD can also increase the displacement of the VD, and thus enhance the energy dissipation efficiency of the damper. It is consistent with the damping enhancement discussed in Fig. 10(a). For the mode shape in regime 2 shown in Fig. 11(b), the mode shape amplitude of the damper decreases as the inertance increases, which implies that the modal damping ratio of the cable would decrease with the increase of the inertance in this regime.

4.3 Modal behavior of the cable with HVID

For the cable with HVID, there are also three distinct regimes of the modal behavior observed in the n^{th} cable mode with the variation of the inertance.

(1) Regime 1 (underdamped modes): when $0 \leq b_h \leq \bar{b}_{h,n}^{opt} T/(\omega_n^0 x_1)$, both the cable undamped frequency and clamped frequency decrease with the increase

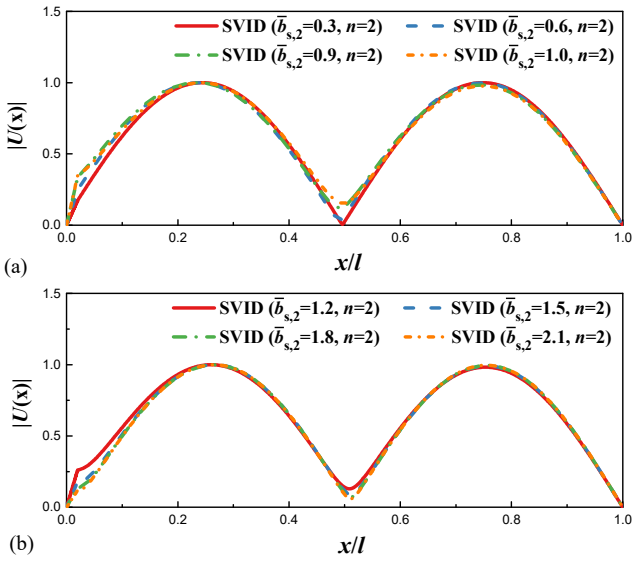

Fig. 11 Mode shapes of the cable with SVID in the second mode (a) regime 1; (b) regime 2

of the inertance, but the optimum cable modal damping ratio increases as the inertance increases.

(2) Regime 2 (underdamped modes): when $\bar{b}_{\mathrm{h},n}^{\mathrm{opt}}T/(\omega_n^0 x_1) \le b_{\mathrm{h}} \le \bar{b}_{\mathrm{h},n-1}^{\mathrm{opt}}T/(\omega_{n-1}^0 x_1)$, mode crossover is observed between the $(n+1)^{\mathrm{th}}$ cable mode and the n^{th} cable mode. The frequency-damping curves originate from its undamped frequency, and terminate at the clamped frequency of the $(n+1)^{\mathrm{th}}$ cable mode or the $(n+2)^{\mathrm{th}}$ cable modes. The cable vibration of the n^{th} cable mode is covered by the $(n+1)^{\mathrm{th}}$ cable mode with a lower damping ratio.

(3) Regime 3 (underdamped modes): when $b_{\mathrm{h}} \ge \bar{b}_{\mathrm{h},n-1}^{\mathrm{opt}}T/(\omega_{n-1}^0 x_1)$, the frequency-damping curves originate from its undamped frequency, and terminate at the clamped frequency of the $(n-1)^{\mathrm{th}}$ cable mode. The cable vibration of the n^{th} cable mode is converted as the $(n-1)^{\mathrm{th}}$ cable mode, and the optimum cable modal damping ratio decreases as the inertance increases.

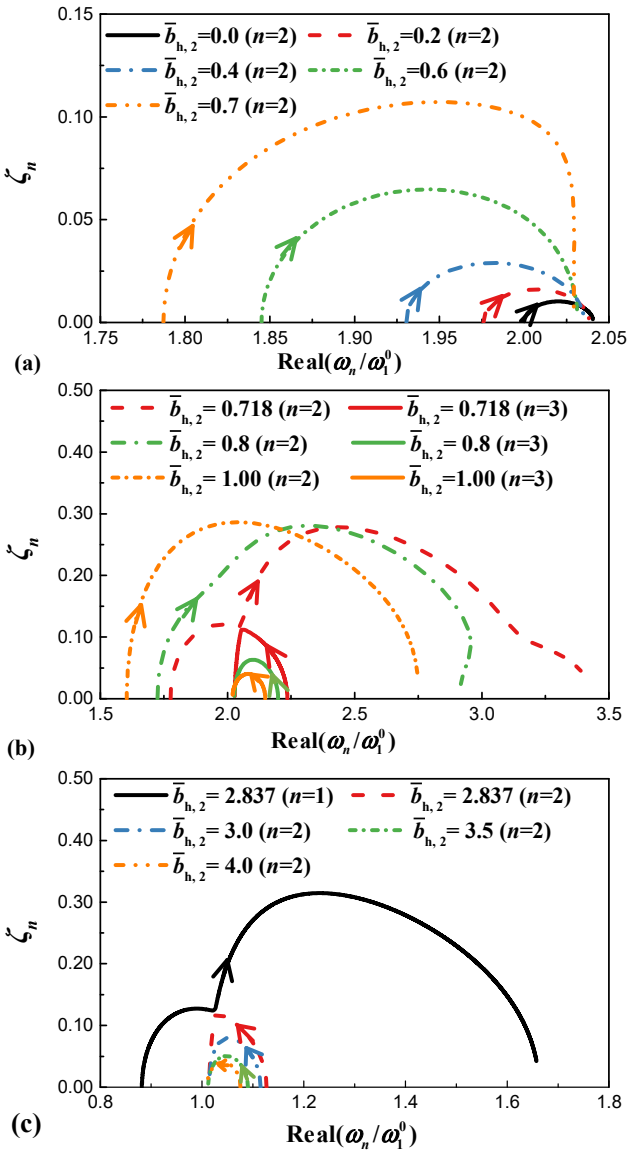

Fig. 12 Frequency-damping evolution curve of cable with HVID in the n^{th} cable mode (a) regime 1; (b) regime 2; (c) regime 3

Above results can be seen in Fig. 12, which shows the modal behavior of the cable with HVID of the 2nd cable mode. It is seen from Fig. 12 that:

(1) When $b_{\mathrm{h}} < \bar{b}_{\mathrm{h},2}^{\mathrm{opt}}T/(\omega_2^0 x_1)$, the cable undamped frequency and the clamped frequency decrease with the increase of the inertance. Compared with the undamped frequency, the inerter has less impact on the clamped frequency. The optimum cable modal damping ratio increases as the inertance increases.

(2) When $\bar{b}_{\mathrm{h},2}^{\mathrm{opt}}T/(\omega_2^0 x_1) \le b_{\mathrm{h}} \le \bar{b}_{\mathrm{h},1}^{\mathrm{opt}}T/(\omega_1^0 x_1)$, mode crossover is observed between the second cable mode and the third cable mode. The frequency-damping evolution curves in the second mode originate from its undamped frequency and terminate at the clamped frequency of third mode or the fourth mode, while these curves in the third mode originate from its undamped frequency and terminate at the clamped frequency of the second mode. The actual vibration of the second cable mode is fully concealed by the third mode. And the third optimum modal damping ratio decreases as the inertance increases.

(3) When $b_{\mathrm{h}} \ge \bar{b}_{\mathrm{h},1}^{\mathrm{opt}}T/(\omega_1^0 x_1)$, mode crossover is observed between the second cable mode and the first cable mode. The frequency-damping evolution curves of the second cable mode originate its undamped frequency and terminate at the clamped frequency of the first cable mode. The cable vibration of the second cable mode is converted as the first cable mode, and the optimum modal damping ratio decreases as the inertance increases.

5. Effect of the inerter in mitigating the multi-mode cable vibrations

5.1 Design strategy targeting at multi-mode cable vibrations

To investigate the effect of the inerter on the control performance of the VD in mitigating multi-mode cable vibrations, the constrained static output LQR method is used to obtain the optimum damping coefficient of the VD for a given inertance of the inerter.

By using the finite difference method, the equation of motion of the cable-VD-inerter system can be described as (Mehrabi and Tabatabai 1998)

$$\boldsymbol{M}_d\ddot{\boldsymbol{u}} + \boldsymbol{K}\boldsymbol{u} = \boldsymbol{f} - \boldsymbol{\gamma}F_{\mathrm{VD}} \tag{26}$$

where $\mathbf{M_d}$ is the mass matrix of the cable that considers the effect of the inerter; $\mathbf{K}$ is the stiffness matrix of the cable; $\mathbf{u}$, $\mathbf{f}$, $\boldsymbol{\gamma}$ are vectors of the displacement, the external

force and the VD position, respectively.

For the case of the cable with PVID or HVID

$$\mathbf{M}_{\mathrm{d}} = ma\mathbf{I}_n + \boldsymbol{\gamma}_{\mathrm{b}} b_\tau \boldsymbol{\gamma}_{\mathrm{b}}^{\mathrm{T}} (\tau = \mathrm{p}, \mathrm{h}),\ \mathbf{K} = \frac{T}{a}\begin{bmatrix} 2 & -1 & & \\ -1 & 2 & \ddots & \\ & \ddots & \ddots & -1 \\ & & -1 & 2 \end{bmatrix} \tag{27}$$

$$\mathbf{u} = [u_1 \quad u_2 \quad \cdots \quad u_n]^{\mathrm{T}},\ \mathbf{f} = [f_1 \quad f_2 \quad \cdots \quad f_n]^{\mathrm{T}}$$

$$\boldsymbol{\gamma} = [\gamma_1 \quad \gamma_2 \quad \cdots \quad \gamma_n]^{\mathrm{T}},\ \boldsymbol{\gamma}_{\mathrm{b}} = [\gamma_{\mathrm{b}1} \quad \gamma_{\mathrm{b}2} \quad \cdots \quad \gamma_{bn}]^{\mathrm{T}}$$

and for the case of the cable with SVID, they are

$$\mathbf{M}_{\mathrm{d}} = \begin{bmatrix} ma\mathbf{I}_n & \\ & b_{\mathrm{s}} \end{bmatrix},\ \mathbf{K} = \frac{T}{a}\begin{bmatrix} 2 & -1 & & & \\ -1 & 2 & \ddots & & \\ & \ddots & \ddots & -1 & \\ & & -1 & 2 & \\ & & & & 0 \end{bmatrix} \tag{28}$$

$$\mathbf{u} = [u_1 \quad u_2 \quad \cdots \quad u_n \quad u_{\mathrm{b}}]^{\mathrm{T}}$$

$$\mathbf{f} = [f_1 \quad f_2 \quad \cdots \quad f_n \quad 0]^{\mathrm{T}}$$

$$\boldsymbol{\gamma} = [\gamma_1 \quad \gamma_2 \quad \cdots \quad \gamma_n \quad -1]^{\mathrm{T}}$$

in which $\mathbf{I}_n$ is an n-dimensional identity matrix; $a = l/(n+1)$ is the length of the discretized cable elements; u_i is the displacement of the cable i^{th} node; f_i is the external force applied on the cable i^{th} node; γ_i and γ_{bi} is determined by the VD and the inerter location. If the damper or the inerter is installed at the j^{th} node of the cable, there is

$$\gamma_i = \begin{cases} 0 & i \neq j \\ 1 & i = j \end{cases} \quad \gamma_{b_i} = \begin{cases} 0 & i \neq j \\ 1 & i = j \end{cases} \tag{29}$$

Using only the velocity of the VD as the feedback, the Eq. (26) can be rewritten in the form of the state space model as

$$\dot{\boldsymbol{Z}}_m = \boldsymbol{A}_m \boldsymbol{Z}_m + \boldsymbol{B}_f \boldsymbol{f} - \boldsymbol{G}_m c_d \boldsymbol{H}_c \boldsymbol{Z}_m \tag{30}$$

where

$$\boldsymbol{Z}_m = \begin{bmatrix} \boldsymbol{u} \\ \dot{\boldsymbol{u}} \end{bmatrix},\ \mathbf{A}_m = \begin{bmatrix} \mathbf{0} & I \\ -\boldsymbol{M}_d^{-1}\boldsymbol{K} & \mathbf{0} \end{bmatrix}$$
$$\boldsymbol{G}_m = \begin{bmatrix} \mathbf{0} \\ \boldsymbol{M}_d^{-1}\boldsymbol{\gamma} \end{bmatrix},\ \boldsymbol{H}_c = [\mathbf{0} \quad \boldsymbol{\gamma}^T] \tag{31}$$

To suprress the cable vibration dominated by the first k modes, the performance index can be expressed as Gao *et al*. (2021)

$$\begin{aligned} J &= E\left[\int_0^\infty \boldsymbol{Z}_m^T \boldsymbol{Q} \boldsymbol{Z}_m + R F_{\mathrm{VD}}^2 dt\right] \\ &= E\left[\int_0^\infty \boldsymbol{Z}_m^T (\boldsymbol{Q} + \boldsymbol{H}_c^T R c^2 \boldsymbol{H}_c) \boldsymbol{Z}_m dt\right] \\ &= \mathrm{trace}(\mathbf{V}_{k+1}^T \boldsymbol{P} \boldsymbol{V}_{k+1}) \end{aligned} \tag{32}$$

where $E[\ ]$ is the mathematical expectation; $\mathbf{Q}$ and R are the weight of the state and the control force, respectively; $\boldsymbol{V}_{k+1}$ is submatrix of the eigenvector matrix $\mathbf{V}$ that contains eigenvectors of the first $(k+1)$ cable modes; $\mathbf{P}$ is determined by the following equation (Agrawal and Yang 1999)

$$\begin{aligned} &(\boldsymbol{A}_m - \boldsymbol{G}_m c \boldsymbol{H}_c)^T \boldsymbol{P} + \boldsymbol{P}(\boldsymbol{A}_m - \boldsymbol{G}_m c \boldsymbol{H}_c) \\ &+ \mathbf{H}_c^T R c^2 \boldsymbol{H}_m + \boldsymbol{Q} = \mathbf{0} \end{aligned} \tag{33}$$

Eqs. (32)-(33) indicate that the damping coeffient of the VD and performance index are dependent on the weight $\mathbf{Q}$ and R. In this study, the weight matrices $\mathbf{Q}$ is taken as

$$\boldsymbol{Q} = \begin{bmatrix} \bar{\boldsymbol{K}} & \\ & \bar{\boldsymbol{M}} \end{bmatrix} \tag{34}$$

where $\bar{\mathbf{K}} = \mathrm{diag}(\mathbf{V}^T \mathbf{K} \mathbf{V})$, $\bar{\mathbf{M}} = \mathrm{diag}(\mathbf{V}^T \mathbf{M_d} \mathbf{V})$.

With the assumption of an initial value of the control force weighting R, the performance index $J(R)$ and optimum damping coefficient can be obtained numerically by using common optimization algorithms, such as the constrained gradient optimization method used in (Agra Agrawal and Yang 1999). However, as R decreases, the performance index also decreases, while the damping coefficient increases (Agrawal and Yang 1999). To balance the control performance and the cost of the damper, the selected R satisfies the following equation

$$[J(R) - J(0.01R)]/J(R) < \varepsilon' \tag{35}$$

where ε' is the given threshold and equals to 0.01 in this study.

After the R is selected, the corresponding performance index and the damping coefficient of the VD for a given inertance are also obtained. Varying the inertance of the inerter, the optimum damping coefficient of VD of the three cases for multi-mode cable vibration control can be obtained according to the relationship between the inertance and $J(R)$.

5.2 Performance evaluation of the VD with the inerter

The NO. A18 stay cable in Sutong Bridge is selected as an example to investigate the effect of the inerter on the control performance of the VD in mitigating multi-mode cable vibrations. Table 2 lists the main properties of the cable. Two design scenarios are considered. One is designed for the first four cable modes, and the other one is designed for the first eight cable modes. In particular, the latter design scenario can cover all the probable modes of wind-rain induced vibrations of the selected cable. During the design, the VD and the inerter of the HVID are respectively installed at 2%l and 3%l from the lower cable end. For the VD, PVID, and SVID, two installed locations are

Table 2 Main properties of the No. A18 cable in the Sutong Bridge

Item	Value
Cable length l	337.43 m
Mass per unit length m	74.02 kg/m
Tension force T	4709 kN

Table 3 Design parameters of the VD and inerter, the minimum and average modal damping ratios of the cable design modes when the first four cable modes are considered

Case	Location	Optimal intertance ratio	Optimal damping coefficient	The average value of modal damping ratios	The minimum value of modal damping ratios
VD	$x_1 = 0.02l$		1.65×10^5	0.887%	0.766%
VD	$x_1 = 0.03l$		1.11×10^5	1.346%	1.161%
PVID	$x_1 = 0.02l$	0.61	1.28×10^5	1.283%	0.860%
PVID	$x_1 = 0.03l$	0.39	8.71×10^4	1.922%	1.288%
SVID	$x_1 = 0.02l$	3.94	2.08×10^5	1.149%	0.741%
SVID	$x_1 = 0.03l$	2.72	1.38×10^5	1.732%	1.114%
HVID	$x_1 = 0.02l$ $x_2 = 0.03l$	0.55	2.05×10^5	2.179%	1.237%

Table 4 Design parameters of the VD and inerter, the minimum and average modal damping ratios of the cable design modes when the first eight cable modes are considered

Case	Location	Optimal intertance ratio	Optimal damping coefficient	The average value of modal damping ratios	The minimum value of modal damping ratios
VD	$x_1 = 0.02l$		1.24×10^5	0.791%	0.564%
VD	$x_1 = 0.03l$		8.25×10^4	1.213%	0.872%
PVID	$x_1 = 0.02l$	0.19	1.08×10^5	0.982%	0.533%
PVID	$x_1 = 0.03l$	0.114	7.31×10^4	1.476%	0.835%
SVID	$x_1 = 0.02l$	3.77	1.41×10^5	0.883%	0.523%
SVID	$x_1 = 0.03l$	2.61	9.24×10^4	1.343%	0.804%
HVID	$x_1 = 0.02l$ $x_2 = 0.03l$	0.18	1.69×10^5	1.856%	0.893%

considered. One is that these dampers are installed at the same location as the VD in HVID, and the other installed location of these dampers is the same as the inerter in HVID.

When the VD of the PVID, SVID and HVID are at installed 2%l from the lower cable end and these dampers are optimized to mitigate the first eight mode cable vibrations, the variation of the performance index and the damping coefficient of the VD with the inertance ratio is plotted in Fig. 13, where the inertance ratio μ is defined as

$$\mu = b_\tau / ml, k = p, \mathrm{s}, \mathrm{h} \tag{36}$$

As shown in Fig. 13, the performance index firstly decreases as the inertance ratio increases, reaching its minimum value at the optimum inertance ratio, and then increases with the increase of the inertance ratio. Similar results can be also found in other design cases. On the basis, Tables 3 and 4 list the design parameters of the VD and inerter, the minimum and average modal damping ratios of the cable design modes. Fig. 14 compares the first eight modal damping ratios of the cable.

As shown in Tables 3-4, the PVID would decrease the optimum damping coefficient of the VD, while the SVID and HVID would increase the optimum damping coefficient of the VD. Compared with other control strategies, the HVID needs a larger damping coefficient to achieve the optimal design, especially for the cases of the VD, PVID,and SVID installed at the same location as the inerter in the HVID. In addition, the optimum inertance and the corresponding damping coefficient tend to decrease as the designed cable mode order increases.

As shown in Fig. 14, when the VD, PVID, and SVID are installed at 2%l from the lower cable end, the HVID generally provides larger modal damping ratios than other dampers in the designed cable modes. When the VD, PVID, and SVID are installed at 3%l from the cable lower end, these dampers could provide larger modal damping ratios to cable in some cable modes. However, Tables 3 and 4 reported that the minimum and average modal damping ratios of the cable design modes of the cable with HVID are larger than other control strategies. Hence, the HVID is considered more effective than the cases when the VD and the inerter are installed at the same location in mitigating cable multi-mode vibrations. In addition, Fig. 14(a) demonstrated that the inerter generally enhances the modal damping ratios provided by the VD in the first four cable modes, while it has an adverse effect on the VD control performance for the cable vibration in the 5^{th}-8^{th} cable modes, especially for the PVID and the HVID. This means that the inerter has an adverse effect on the VD performance for the cable mode order beyond the design range.

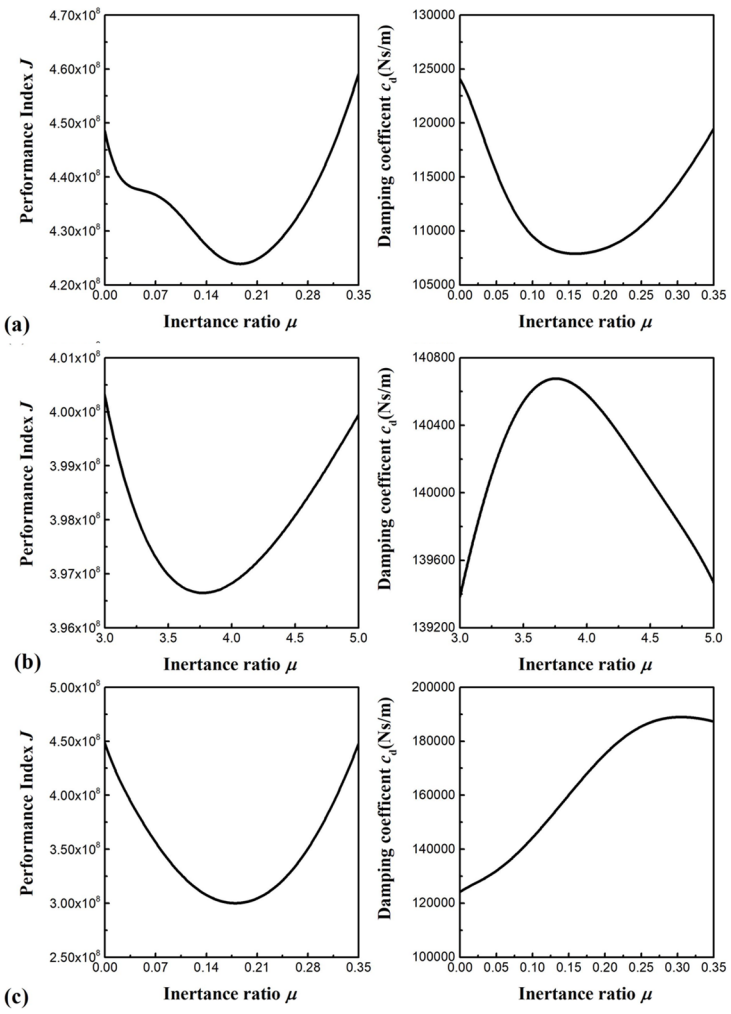

Fig. 13 Performance index and damping coefficient of VD as a function of the inertance ratio when the first eight cable modes are considered (a) PVID; (b) SVID (c) HVID

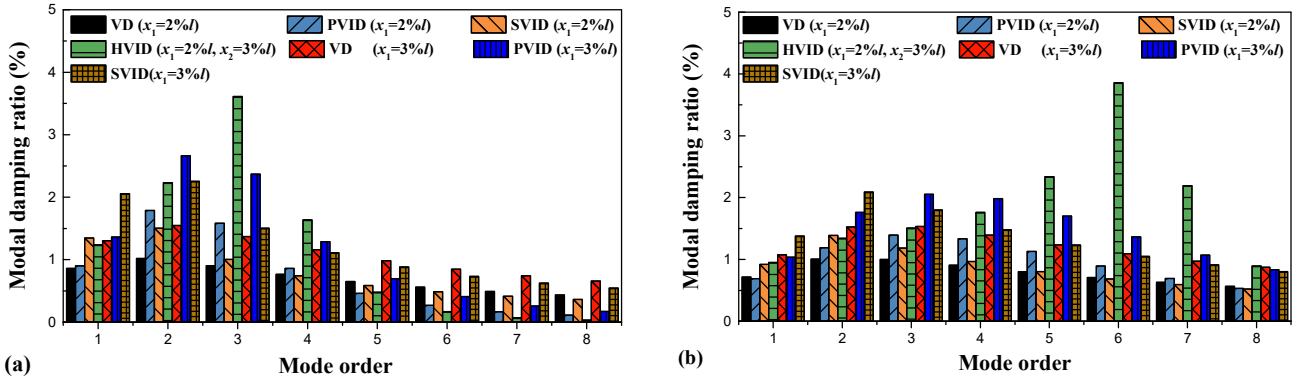

Fig. 14 Comparison of the cable modal damping ratios in the first eight cable modes (a) design the first four cable modes; (b) design the first eight cable modes

6. Conclusions

This paper systematically investigated the effects of the inerter on the cable oscillation frequency, the attainable modal damping ratio, and the control performance in mitigating multi-mode cable vibrations. The conclusions are summarized as follows.

- The modal behaviors of the cable with PVID and HVID can be divided into three regimes with the variation of the inertance. In the first regime, the inerter can increase the achievable modal damping ratio of the cable, and achieve better control performance with the increase of inertance. In the second and third regimes, cable mode crossover is

observed and the optimum modal damping ratio of the cable decreases with the increase of the inertance.

- Only two regimes of modal behaviors can be observed for the cable with the SVID. In the first regime, better control performance can be achieved with the increase of inertance. However, the inerter has an adverse effect on the VD performance when the dimensionless inertance is less than 0.5. In the second regime, the optimum modal damping ratio of the cable decreases with the increase of the inertance, but is always larger than the optimum modal damping ratio provided by VD. Compared with the PVID and HVID, the SVID needs lager inertance and damping coefficient to improve the VD performance.
- The inerter generally enhances the modal damping ratio in multiple cable modes, but has an adverse effect on the VD performance for the cable mode order beyond the design range, especially for the PVID and the HVID. Compared with the cases when the VD and the inerter are installed at the same location, the HVID can achieve better control performance in mitigating multi-mode cable vibrations. However, the HVID needs a larger damping coefficient than other control strategies, especially for the cases the VD, PVID, and SVID installed at the same location as the inerter in the HVID.

Acknowledgments

The authors greatly acknowledge the financial support from the National Natural Science Foundation of China (51722804, 51878274, 51978155), the National Ten Thousand Talent Program for Young Top-notch Talents (W03070080), and the Project of Scientific Research and Development Plan of China-railway.

References

Agrawal, A.K. and Yang, J.N. (1999), "Design of passive energy dissipation systems based on LQR control methods", *J. Intell. Mater. Syst. Struct.*, **10**(12), 933-944. https://doi.org/10.1106/FB58-N1DG-ECJT-B8H4

Ahmad, J., Cheng, S.H. and Ghrib, F. (2018), "Combined effect of external damper and cross-tie on the modal response of hybrid two-cable networks", *J. Sound Vib.*, **417**, 132-148. https://doi.org/10.1016/j.jsv.2017.12.023

Cai, C.S., Wu, W.J. and Araujo, M. (2007), "Cable vibration control with a TMD-MR damper system: experimental exploration", *J. Struct. Eng.*, **133**(5), 629-637. https://doi.org/10.1061/(ASCE)0733-9445(2007)133:5(629)

Chen, Z.Q., Wang, X.Y., Ko, J.M., Ni, Y.Q., Spencer, B.F., Yang, G. and Hu, J.H. (2004), "MR damping system for mitigating wind-rain induced vibration on Dongting Lake Cable-Stayed Bridge", *Wind Struct., Int. J.*, **7**(5), 293-304. https://doi.org/10.12989/was.2004.7.5.293

Chen, L., Sun, L.M. and Nagarajaiah, S. (2015), "Cable with discrete negative stiffness device and viscous damper: passive realization and general characteristics", *Smart Struct. Syst., Int. J.*, **15**(3), 627-643. http://dx.doi.org/10.12989/sss.2015.15.3.627

Chen, L., Nagarajaiah, S. and Sun, L.M. (2021), "A unified analysis of negative stiffness dampers and inerter-based absorbers for multimode cable vibration control", *J. Sound Vib.*, 494: 115814. https://doi.org/10.1016/j.jsv.2020.115814

Christenson, R.E., Spencer, B.F. and Johnson, E.A. (2006), "Experimental verification of smart cable damping", *J. Eng. Mech.*, **132**(3), 268-278. https://doi.org/10.1061/(ASCE)0733-9399(2006)132:3(268)

Domenico, D.D. and Ricciardi, G. (2019), "An enhanced base isolation system equipped with optimal tuned mass damper inerter (TMDI)", *Earthq. Eng. Struct. D.*, **47**(5), 1169-1192. https://doi.org/10.1002/eqe.3011

Duan, Y.F., Ni, Y.Q. and Ko, J.M. (2005), "State-derivative feedback control of cable vibration using semiactive magnetorheological dampers", *Comput-Aided. Civ. Inf.*, **20**(6), 431-449. https://doi.org/10.1111/j.1467-8667.2005.00396.x

Duan, Y., Ni, Y.Q., Zhang, H., Spencer Jr, B.F., Ko, J.M. and Dong, S. (2019), "Design formulas for vibration control of sagged cables using passive MR dampers", *Smart Struct. Syst., Int. J.*, **23**(6), 537-551. https://doi.org/10.12989/sss.2019.23.6.537

Fournier, J.A. and Cheng, S.H. (2014), "Impact of damper stiffness and damper support stiffness on the efficiency of a linear viscous damper in controlling stay cable vibrations", *J. Bridge Eng.*, **19**(4), 04013022. https://doi.org/10.1061/(ASCE)BE.1943-5592.0000562

Fujino, Y. and Hoang, N. (2008), "Design formulas for damping of a stay cable with a damper", *J. Struct. Eng.*, **134**(2), 269-278. https://doi.org/10.1061/(ASCE)0733-9445(2008)134:2(269)

Gao, H., Wang, H., Li, J., Wang, Z., Liang, R., Xu, Z. and Ni, Y. (2021), "Optimum design of viscous inerter damper targeting multi-mode vibration mitigation of stay cables", *Eng. Struct.*, **226**, 111375. https://doi.org/10.1016/j.engstruct.2020.111375

Giaralis, A. and Petrini, F. (2017), "Wind-induced vibration mitigation in tall buildings using the tuned mass-damper-inerter", *J. Struct. Eng.*, **143**(9), 04017127. https://doi.org/10.1061/(ASCE)ST.1943-541X.0001863

He, X., Cai, C., Wang, Z., Jing, H. and Qin, C. (2018), "Experimental verification of the effectiveness of elastic cross-ties in suppressing wake-induced vibrations of staggered stay cables", *Eng. Struct.*, **167**, 151-165. https://doi.org/10.1016/j.engstruct.2018.04.033

Hoang, N. and Fujino, Y. (2008), "Combined damping effect of two dampers on a stay cable", *J. Bridge Eng.*, **13**(3), 299-303. https://doi.org/10.1061/(ASCE)1084-0702(2008)13:3(299)

Hu, Y., Chen, M.Z., Shu, Z. and Huang, L. (2015), "Analysis and optimisation for inerter-based isolators via fixed-point theory and algebraic solution", *J. Sound Vib.*, **346**, 17-36. https://doi.org/10.1016/j.jsv.2015.02.041

Huang, H.W., Liu, T.T. and Sun, L.M. (2019a), "Multi-mode cable vibration control using MR damper based on nonlinear modeling", *Smart Struct. Syst., Int. J.*, **23**(6), 565-577. https://doi.org/10.12989/sss.2019.23.6.565

Huang, Z., Hua, X., Chen, Z. and Niu, H. (2019b), "Performance evaluation of inerter-based damping devices for structural vibration control of stay cables", *Smart Struct. Syst., Int. J.*, **23**(6), 615-626. https://doi.org/10.12989/sss.2019.23.6.615

Ikago, K., Saito, K. and Inoue, N. (2012), "Seismic control of single-degree-of-freedom structure using tuned viscous mass damper", *Earthq. Eng. Struct. D.*, **41**(3), 453-474. https://doi.org/10.1002/eqe.1138

Jamshidi, M., Chang, C.C. and Bakhshi, A. (2017), "Self-powered hybrid electromagnetic damper for cable vibration mitigation", *Smart Struct. Syst., INt. J.*, **20**(3), 285-301. https://doi.org/10.12989/sss.2017.20.3.285

Javanbakht, M., Cheng, S.H. and Ghrib, F. (2020), "Multimode

vibration control of stay cables using optimized negative stiffness damper", *Struct. Control Health Monit.*, **27**(4), e2503. https://doi.org/10.1002/stc.2503

Jeong, S., Lee, J., Cho, S. and Sim, S.H. (2019), "Integrated cable vibration control system using Arduino", *Smart Struct. Syst., Int. J.*, **23**(6), 695-702. https://doi.org/10.12989/sss.2019.23.6.695

Johnson, E.A., Christenson, R.E. and Spencer, B.F. (2003), "Semiactive damping of cables with sag", *Comput-Aided. Civil Inf.*, **18**(2), 132-146. https://doi.org/10.1111/1467-8667.00305

Jung, H.J., Spencer Jr, B.F., Ni, Y.Q. and Lee, I.W. (2004), "State-of-the-art of semiactive control systems using MR fluid dampers in civil engineering applications", *Struct. Eng. Mech., Int. J.*, **17**(3-4), 493-526. https://doi.org/10.12989/sem.2004.17.3_4.493

Kim, I.H., Jung, H.J. and Koo, J.H. (2010), "Experimental evaluation of a self-powered smart damping system in reducing vibrations of a full-scale stay cable", *Smart Mater. Struct.*, **19**(11), 115027. https://doi.org/10.1088/0964-1726/19/11/115027

Kleissl, K. and Georgakis, C.T. (2012), "Comparison of the aerodynamics of bridge cables with helical fillets and a pattern-indented surface", *J. Wind Eng. Ind. Aerod.*, **104**, 166-175. https://doi.org/10.1016/j.jweia.2012.02.031

Kovacs, I. (1982), "Zur frage der seilschwingungen und der seildampfung", *Die Bautechnik.*, **59**, 325-32. [In German]

Krenk, S. (2000), "Vibrations of a taut cable with an external damper", *J. Appl. Mech.*, **67**(4), 772-776. https://doi.org/10.1115/1.1322037

Lazar, I.F., Neild, S.A. and Wagg, D.J. (2014), "Using an inerter-based device for structural vibration suppression", *Earthq. Eng. Strut. D.*, **43**(8), 1129-1147. https://doi.org/10.1002/eqe.2390

Lazar, I.F., Neild, S.A. and Wagg, D.J. (2016), "Vibration suppression of cables using tuned inerter dampers", *Eng. Struct.*, **122**, 62-71. https://doi.org/10.1016/j.engstruct.2016.04.017

Li, H., Liu, M. and Ou, J.P. (2008), "Negative stiffness characteristics of active and semi-active control systems for stay cables", *Struct. Control Health Monit.*, **15**(2), 120-142. https://doi.org/10.1002/stc.200

Li, S., Chen, Z., Wu, T. and Kareem, A. (2013), "Rain-wind-induced in-plane and out-of-plane vibrations of stay cables", *J. Eng. Mech.*, **139**, 1688-1698. https://doi.org/10.1061/(ASCE)EM.1943-7889.0000612

Li, Y.M., Shen, W.A. and Zhu, H.P. (2019), "Vibration mitigation of stay cables using electromagnetic inertial mass dampers: full-scale experiment and analysis", *Eng. Struct.*, **200**, 109693. https://doi.org/10.1016/j.engstruct.2019.109693

Li, J.Y., Zhu, S., Shi, X. and Shen, W. (2020), "Electromagnetic shunt damper for bridge cable vibration mitigation: full-scale experimental study", *J. Struct. Eng.*, **146**(1), 04019175. https://doi.org/10.1061/(ASCE)ST.1943-541X.0002477

Liu, M., Yang, W., Chen, W. and Li, H. (2019), "Experimental investigation on multi-mode vortex-induced vibration control of stay cable installed with pounding tuned mass dampers", *Smart Struct. Syst., Int. J.*, **23**(6), 579-587. https://doi.org/10.12989/sss.2019.23.6.579

Lu, L., Duan, Y.F., Spencer Jr, B.F., Lu, X. and Zhou, Y. (2017), "Inertial mass damper for mitigating cable vibration", *Struct. Control Health Monit.*, **24**(10), e1986. https://doi.org/10.1002/stc.1986

Lu, L., Fermandois, G.A., Lu, X., Spencer Jr, B.F., Duan, Y.F. and Zhou, Y. (2019), "Experimental evaluation of an inertial mass damper and its analytical model for cable vibration mitigation", *Smart Struct. Syst., Int. J.*, **23**(6), 589-613. https://doi.org/10.12989/sss.2019.23.6.589

Luo, J.N., Jiang, J.Z. and Macdonald, J.H.G. (2019), "Cable vibration suppression with inerter-based absorbers", *J. Eng. Mech.*, **145**(2), 04018134. https://doi.org/10.1061/(ASCE)EM.1943-7889.0001554

Main, J.A. and Jones, N.P. (2002), "Free vibrations of taut cable with attached damper. I: Linear viscous damper", *J. Eng. Mech.*, **128**(10), 1062-1071. https://doi.org/10.1061/(ASCE)0733-9399(2002)128:10(1062)

Mehrabi, A.B. and Tabatabai, H. (1998), "Unified finite difference formulation for free vibration of cables", *J. Struct. Eng.*, **124**(11), 1313-1322. https://doi.org/10.1061/(ASCE)0733-9445(1998)124:11(1313)

Ma, R.S., Bi, K.M. and Hao, H. (2020), "Using inerter-based control device to mitigate heave and pitch motions of semi-submersible platform in the shallow sea", *Eng. Struct.*, **207**, 110248. https://doi.org/10.1016/j.engstruct.2020.110248

Ma, R.S., Bi, K.M., Hao, H. (2021), "A novel rotational inertia damper for amplifying fluid resistance: Experiment and mechanical model", *Mech. Syst. Signal PR.*, **149**, 107313. https://doi.org/10.1016/j.ymssp.2020.107313

Marian, L. and Giaralis, A. (2014), "Optimal design of a novel tuned mass-damper–inerter (TMDI) passive vibration control configuration for stochastically support-excited structural systems", *Probabilist. Eng. Mech.*, **38**, 156-164. https://doi.org/10.1016/j.probengmech.2014.03.007

Nakamura, Y., Fukukita, A., Tamura, K., Yamazaki, I., Matsuoka, T., Hiramoto, K. and Sunakoda, K. (2014), "Seismic response control using electromagnetic inertial mass dampers", *Earthq. Eng. Struct. D.*, **43**(4), 507-527. https://doi.org/10.1002/eqe.2355

Ni, Y.Q., Wang, X.Y., Chen, Z.Q. and Ko, J.M. (2007), "Field observations of rain-wind-induced cable vibration in cable-stayed Dongting Lake Bridge", *J. Wind Eng. Ind. Aerod.*, **95**(5), 303-328. https://doi.org/10.1016/j.jweia.2006.07.001

Pacheco, B.M., Fujino, Y. and Sulekh, A. (1993), "Estimation curve for modal damping in stay cables with viscous damper", *J. Struct. Eng.*, **119**(6), 1961-1979. https://doi.org/10.1061/(ASCE)0733-9445(1993)119:6(1961)

Shen, X., Ma, R.J., Ge, C.X. and Hu, X.H. (2018), "Long-term monitoring of super-long stay cables on a cable-stayed bridge", *Wind Struct., Int. J.*, **27**(6), 357-368. https://doi.org/10.12989/was.2018.27.6.357

Shi, X. and Zhu, S.Y. (2018), "Dynamic characteristics of stay cables with inerter dampers", *J. Sound Vib.*, **423**, 287-305. https://doi.org/10.1016/j.jsv.2018.02.042

Shi, X., Zhu, S., Li, J.Y. and Spencer, B.F. (2016), "Dynamic behavior of stay cables with passive negative stiffness dampers", *Smart Mater. Struct.*, **25**(7), 075044. https://doi.org/10.1088/0964-1726/25/7/075044

Shi, X., Zhu, S.Y. and Spencer, B.F. (2017), "Experimental study on passive negative stiffness damper for cable vibration mitigation", *J. Eng. Mech.*, **143**(9), 04017070. https://doi.org/10.1061/(ASCE)EM.1943-7889.0001289

Smith, M.C. (2002), "Synthesis of mechanical networks: the inerter", *Ieee. T. On. Automat. Contr.*, **47**(10), 1648-1662. https://doi.org/10.1109/TAC.2002.803532

Sun, L.M., Hong, D.X. and Chen, L. (2017), "Cables interconnected with tuned inerter damper for vibration mitigation", *Eng. Struct.*, **151**, 57-67. https://doi.org/10.1016/j.engstruct.2017.08.009

Wang, X.Y., Ni, Y.Q., Ko, J.M. and Chen, Z.Q. (2005), "Optimal design of viscous dampers for multi-mode vibration control of bridge cables", *Eng. Struct.*, **27**(5), 792-800. https://doi.org/10.1016/j.engstruct.2004.12.013

Wang, Z.H., Xu, Y.W., Gao, H., Chen, Z.Q., Xu, K. and Zhao, S.B. (2019), "Vibration control of a stay cable with a rotary electromagnetic inertial mass damper", *Smart Struct. Syst., Int. J.*, **23**(6), 627-639. https://doi.org/10.12989/sss.2019.23.6.627

Wang, H., Mao, J.X. and Xu, Z.D. (2020), "Investigation of dynamic properties of a long-span cable-stayed bridge during typhoon events based on structural health monitoring", *J. Wind Eng. Ind. Aerod.*, **201**, 104172. https://doi.org/10.1016/j.jweia.2020.104172

Weber, F. and Distl, H. (2015), "Semi-active damping with negative stiffness for multi-mode cable vibration mitigation: approximate collocated control solution", *Smart Mater. Struct.*, **24**(11), 115015. https://doi.org/10.1088/0964-1726/24/11/115015

Weber, F., Feltrin, G., Maślanka, M., Fobo, W. and Distl, H. (2009), "Design of viscous dampers targeting multiple cable modes", *Eng. Struct.*, **31**(11), 2797-2800. https://doi.org/10.1016/j.engstruct.2009.06.020

Zhang, R., Ni, Y.Q., Duan, Y. and Ko, J.M. (2019), "Development of a full-scale magnetorheological damper model for open-loop cable vibration control", *Smart Struct. Syst., Int. J.*, **23**(6), 553-564. https://doi.org/10.12989/sss.2019.23.6.553

Zhang, R., Zhao, Z., Pan, C., Ikago, K. and Xue, S. (2020), "Damping enhancement principle of inerter system", *Struct. Control Health Monit.* **27**(5), e2523. https://doi.org/10.1002/stc.2523

Zhou, P. and Li, H. (2016), "Modeling and control performance of a negative stiffness damper for suppressing stay cable vibrations", *Struct. Control Health Monit.*, **23**(4), 764-782. https://doi.org/10.1002/stc.1809

Zhou, H., Huang, X., Xiang, N., He, J., Sun, L. and Xing, F. (2018a), "Free vibration of a taut cable with a damper and a concentrated mass", *Struct. Control Health Monit.*, **25**(11), e2251. https://doi.org/10.1002/stc.2251

Zhou, H., Xiang, N., Huang, X., Sun, L., Xing, F. and Zhou, R. (2018b), "Full-scale test of dampers for stay cable vibration mitigation and improvement measures", *Struct. Monit. Maint., Int. J.*, **5**(4), 489-506. https://doi.org/10.12989/smm.2018.5.4.489

Zhu, H., Li, Y., Shen, W. and Zhu, S. (2019), "Mechanical and energy-harvesting model for electromagnetic inertial mass dampers", *Mech. Syst. Signal PR.*, **120**, 203-220. https://doi.org/10.1016/j.ymssp.2018.10.023

Appendix A. The determination equation of η_{cr}

The characteristic equation in Eq. (7) for the case of PVID can be expanded into the real and the imaginary part, where the real part is expressed as

$$\frac{\sin(2\sigma x_1)}{cos(2\sigma x_1) - cosh(2\nu x_1)} + \frac{\sin(2\sigma x_2)}{cos(2\sigma x_2^*) - cosh(2\nu x_2^*)} = \frac{-b_p}{m}\sigma \tag{A1}$$

while the imaginary part is

$$\frac{\sinh(2\nu x_1)}{cos(2\sigma x_1) - cosh(2\nu x_1)} + \frac{\sinh(2\nu x_2^*)}{cos(2\sigma x_2^*) - cosh(2\nu x_2^*)} - \frac{b_p}{m}\nu + \eta = 0 \tag{A2}$$

in which $\sigma = \text{Real}(\beta), \nu = Imag(\beta)$

When $\sigma = 0$ the damping ratio is equal to 1, and the solution of β corresponds to the nonoscillatory, exponentially decaying solutions in time. Eq. (A.2) reduces to

$$\frac{\sinh(2\nu x_1)}{1 - cosh(2\nu x_1)} + \frac{\sinh(2\nu x_2^*)}{1 - cosh(2\nu x_2^*)} - \frac{b_p}{m}\nu + \eta = 0 \tag{A3}$$

The determination equation of η_{cr} can be expressed as

$$\eta_{\text{cr}} = \frac{b_p}{m}\nu - \frac{\sinh(2\nu x_1)}{1 - cosh(2\nu x_1)} - \frac{\sinh(2\nu x_2^*)}{1 - cosh(2\nu x_2^*)} \tag{A4}$$